Earthquake Resistant Performance of Prestressed Reinforced Concrete Beam-Column Subassemblages Forming Beam Yield Mechanism

KITAYAMA Kazuhiro
Tokyo Metropolitan University, Japan

YAJIMA Ryuto
Taisei Corporation, Japan

15 WCEE
LISBOA 2012

SUMMARY:
Seismic performance for prestressed reinforced concrete frames forming beam yield mechanism was studied by static loading tests using cruciform beam-column subassemblage specimens. Good bond along beam longitudinal bars within a beam-column joint resulted in fat spindle-shaped hysteresis loops, whereas poor bond resulted in pinching loops like a reinforced concrete structure. The greater a contribution ratio of PC tendons to ultimate flexural capacity of a beam section was, the smaller a beam residual deformation was. A ratio of residual flexural crack width to that at the loading peak was approximately 0.5 which is as much as that for R/C members when the contribution ratio of PC tendons to ultimate flexural capacity was 0.45, whereas the residual ratio of crack width reduced to 0.14 when the contribution ratio of PC tendons was 0.79. A plastic hinge length, different limit states for a beam and energy dissipating capacity were discussed through test results.

Keywords: Earthquake resistance, Prestressed reinforced concrete, Beam-column subassemblage, Beam yield

1. INTRODUCTION

Performance-based design for earthquake resistance of buildings is demanded in the world, which can control structural behaviour of each member and a whole building during earthquakes. It is necessary to evaluate a force-deformation envelope curve and hysteresis loops of a member and grasp damage levels in a member in order to establish performance-based earthquake resistant design methodology. There is, however, few experimental data available to develop such the performance-based design methodology for prestressed reinforced concrete (PRC) buildings because earthquake resistant performance of PRC members changes remarkably with full variety of arrangement of steel bars and PC tendons, depending on bond condition along such longitudinal reinforcement surrounded by concrete or grout mortar.

Therefore, four PRC interior beam-column subassemblage specimens which were designed to form beam yielding mechanism were tested under static load reversals to investigate seismic performance, i.e., hysteretic characteristics, bond along beam longitudinal reinforcement, a plastic hinge length, residual crack width, different limit states for beams and energy dissipating capacity.

2. OUTLINE OF TEST

2.1. Specimens

Four half-scale prestressed reinforced concrete interior beam-column subassemblages, removed from a plane frame by cutting off the beams and columns at arbitrarily assumed inflection points, were tested. A configuration of specimens, section dimensions and reinforcement details are shown in Figure 2.1. Properties of specimens and material properties of concrete, grout mortar and steel are listed in Table 2.1 and 2.2 respectively. Section dimensions, compressive strength of concrete and grout mortar, and

Table 2.1. Properties of specimens

Specimen	Y-1	Y-2	Y-3	Y-4
Concrete compressive strength	68.8 MPa			
Concrete tensile strength	3.1 MPa			
Grout mortar compressive strength	70.3 MPa			
Beam PC strand	2-ϕ12.7 (SWPR7BL)	2-ϕ12.7 (SWPR7BL)	2-ϕ15.2 (SWPR7BL)	4-ϕ12.7 (SWPR7BL)
Ratio of post-tensioning load of PC strand to specified yielding load	0.73	0.74	0.73	0.72
Sheath tube	#1032	#1032	#1035	#1032
Beam top bar	2-D13	2-D19	2-D13	2-D13
Grade of steel	SD295A	SD345	SD295A	SD295A
Beam bottom bar	2-D13	2-D19	2-D13	2-D13
Grade of steel	SD295A	SD345	SD295A	SD295A
Index q_{pr} *1	0.04	0.04	0.06	0.08
Prestressing ratio, λ *2	0.67	0.45	0.73	0.79
Axial stress ratio to column (Axial load)	0.1 (870kN)			

*1 $q_{pr}=(T_{py}+T_{po}+T_{ry}-C_{ry})\ /\ bD\sigma_B$, refer to Equation (4.1).

*2 $\lambda=M_p/\ (M_p+M_r)$

where, Mp : moment contribution of PC strands to ultimate flexural capacity of a beam section and Mr : moment contribution of beam longitudinal bars to ultimate flexural capacity of a beam section.

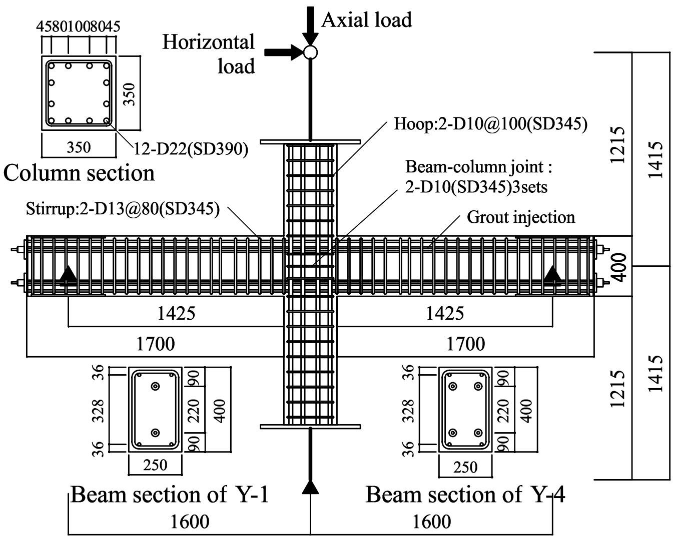

Figure 2.1. Details of specimens

Table 2.2. Material properties of PC strands and steel

Steel	Yield strength MPa	Young Modulus GPa	Yield strain %	Elastic limit strain %
PC strand, ϕ12.7	1742	213	1.02	0.68
PC strand, ϕ15.2	1746	210	1.03	0.69
D10 (SD345)	379	180	0.21	-
D13 (SD295A)	357	187	0.19	-
D13 (SD345)	349	180	0.19	-
D19 (SD345)	397	194	0.20	-
D22 (SD390)	469	196	0.24	-

Note: Yield strength and yield strain for PC strands were determined by the 0.2 % offset method.

specified yield strength, a diameter and a number of column longitudinal bars; 12-D22(SD390), were common for all specimens. The column with a square cross section of 350 mm width had hoops of 2-D10(SD345) at center-to-center spacing of 100 mm. The beam had width of 250 mm and depth of 400 mm with stirrups of 2-D13(SD345) at center-to-center spacing of 80 mm. The length from a center of the column to a support of the beam end was 1600 mm. The height from a center of the beam to the loading point at the top of the column or to the bottom support was 1415 mm respectively. Specimens were designed to form beam collapse mechanism prior to column yielding and shear failure of a beam-column joint.

A combination between a diameter of a non-prestressed longitudinal bar and a kind and a number of a PC tendon in a beam were chosen as a test parameter. Specimen Y-1 was a control specimen, whose

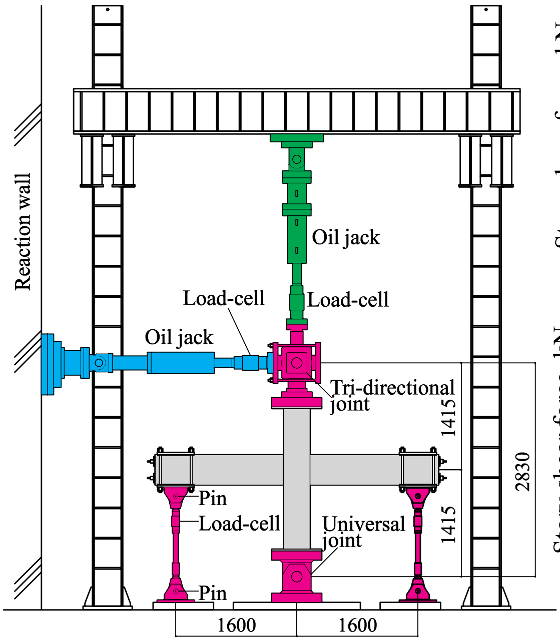

Figure 2.2. Loading apparatus

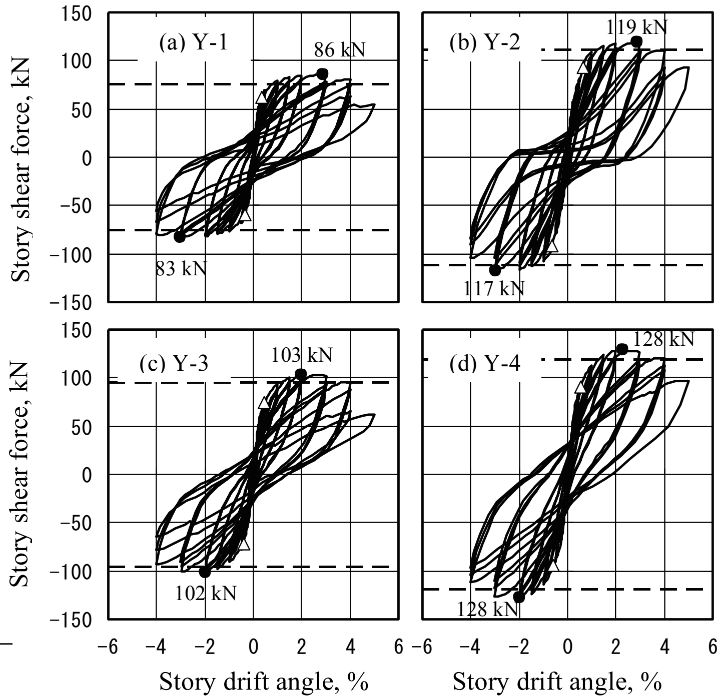

Figure 3.1. Story shear – story drift angle relationships

beam section had two deformed bars with a diameter of 13 mm and a specified strength of 295 N/mm^2, designated as 2-D13 (SD295A), as top and bottom reinforcing bars each and one PC strand consisting of seven steel wires with a whole diameter of 12.7 mm, designated as 1-ϕ12.7 (SWPR7BL), placed each at a top and bottom of the section. Specimen Y-2 had a same PC strand as Specimen Y-1, but different beam reinforcement, i.e., 2-D19 (SD345). Specimen Y-3 had same beam reinforcement as Specimen Y-1, but a different diameter of a PC strand, i.e., 1-ϕ15.2 (SWPR7BL). Specimen Y-4 had same beam reinforcement as Specimen Y-1, but two PC strands, i.e., 2-ϕ12.7 (SWPR7BL), placed each at a top and bottom of the section. A contribution ratio of PC tendons to ultimate flexural capacity of a PRC beam section, called the prestressing ratio hereafter, ranged from 0.45 to 0.79.

PC tendons which passed through beams and a beam-column joint were contained within a sheath tube and post-tensioned up to the desired level of approximately 0.73 times the yield strength of the strand after the concrete gained sufficient strength. Hereafter, grout mortar was injected into the sheath tube. Concrete was cast in upright position. Compressive strength of concrete and grout mortar was 69 N/mm^2 and 70 N/mm^2 respectively.

2.2. Loading Apparatus and Instrumentation

A loading apparatus is shown in Figure 2.2. The beam ends were supported by horizontal rollers, while the bottom of the column was supported by a universal joint. The reversed cyclic horizontal load and the constant axial load in compression (an axial load ratio of 0.10) were applied at the top of the column through a tri-directional joint by three oil jacks. The jack orthogonal to a horizontal loading direction prevented an out-of-plane overturn for a specimen.

Specimens were controlled by a story drift angle for one loading cycle of 0.25 %, two cycles of 0.5 %, three cycles of 1 %, 1.5 %, 2 %, 3 % and 4 % respectively, and one-way loading to 5 %. The story drift angle was defined as a story drift divided by a height of the column; 2830 mm. Lateral force, column axial load and beam shear forces were measured by load-cells. Story drift, beam and column deflections, and local displacement of a beam-column joint were measured by displacement transducers. Strains of tendons, beam bars and column bars were measured by strain gauges.

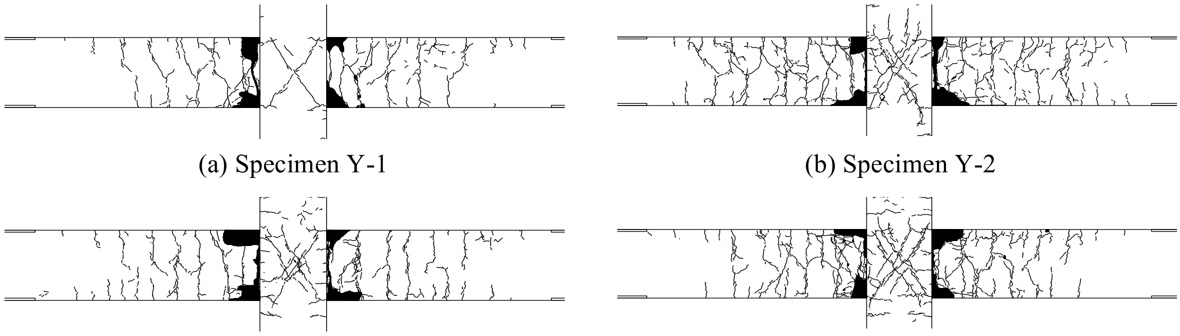

(a) Specimen Y-1 (b) Specimen Y-2

(c) Specimen Y-3 (d) Specimen Y-4

Figure 3.2. Crack patterns at end of test

3. TEST RESULTS

3.1. Story Shear – Drift Relationships

Relationships between the story shear force and the story drift angle are shown in Figure 3.1. The story shear force was obtained from moment equilibrium between measured beam shear forces and the horizontal force at a loading point on the top of the column. Yielding of beam longitudinal bars and a peak of the story shear force are indicated by an open triangle and a solid circle symbol respectively. The theoretical ultimate flexural capacity of the beam is shown by a horizontal dashed line, which was computed by a section analysis assuming that a plane section remains plane and the ideal bond between beam reinforcing steels and surrounding concrete or grout mortar exists.

Beam longitudinal bars for all specimens yielded at a story drift angle of 0.3 % to 0.6 %. The peak story shear force was attained at a story drift angle of 3 % approximately for Specimens Y-1 and Y-2 and 2 % approximately for Specimens Y-3 and Y-4. Specimens Y-1, Y-3 and Y-4, using deformed 13 mm diameter bars as beam longitudinal reinforcement, showed first origin-oriented hysteresis loops, but then spindle-shaped loops with an increase in a story drift. After the peak strength, the story shear force declined for these three specimens due to concrete crushing at beam ends and the buckling and the rupture of beam longitudinal bars. Specimen Y-2, using deformed 19 mm diameter bars as beam longitudinal reinforcement, showed origin-oriented hysteresis loops up to a story drift angle of 0.5 %, but developed hereafter high unloading stiffness as is observed in reinforced concrete members, and eventually exhibited inverted-S-shaped pinching loops. The peak story shear force for all specimens exceeded the ultimate flexural capacity of the beam predicted by the section analysis.

3.2. Crack Patterns

Crack patterns at the end of a test are shown in Figure 3.2. Beam flexural cracks occurred and these cracks grew into diagonal shear cracks with the increase in the deformation. Beam flexural cracks occurred in a narrower region for Specimen Y-1, which had the least beam flexural capacity among specimens, than other specimens. Beams had the greatest number of flexural and shear cracks for Specimen Y-2, which had deformed 19 mm diameter beam bars and whose prestressing ratio was 0.45 the smallest among specimens. Development and growth of flexural or shear cracks in beams were reduced by spall-off and crushing of compressed concrete at a beam end for all specimens, which eventually resulted in exposure of beam longitudinal bars. Diagonal cracks crossing each other developed in the beam-column joint under cyclic reversed loading, but the widths were fine. Joint shear distortion was very small, less than 0.3 %.

3.3. Failure Mode

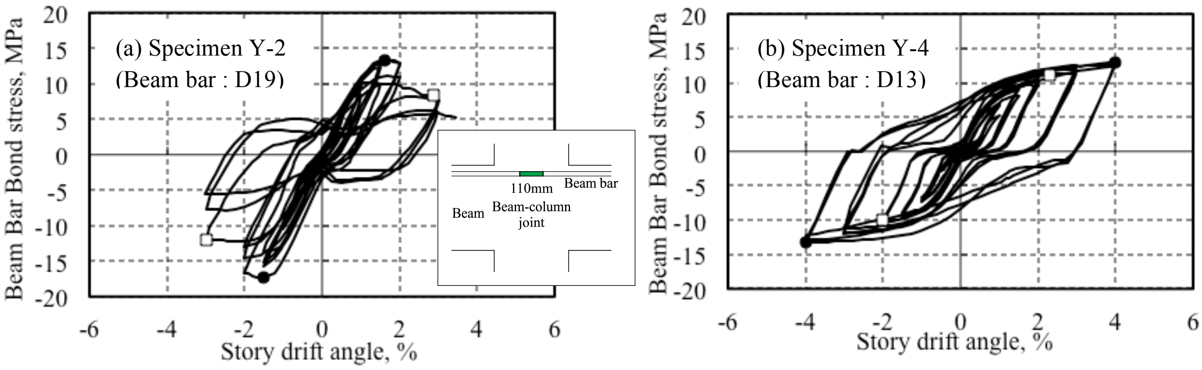

Figure 4.1. Local bond stress along beam bar within beam-column joint

Strains in prestressing strands were not measured because of poor curing of strain gauges attached on the surface of the strands. It is, however, judged that prestressing strands yielded from the fact that the peak bending moment of a beam attained by the test exceeded the ultimate flexural capacity predicted by the section analysis. Peak strength for all specimens was reached after the yielding of beam longitudinal bars and prestressing strands. Lateral capacity declined due to concrete crushing at a beam end and the buckling and the rupture of 13 mm diameter beam bars for Specimens Y-1, Y-3 and Y-4, and only concrete crushing at a beam end for Specimen Y-2 using 19 mm diameter beam bars. Column longitudinal bars did not yield for all specimens.

4. DISCUSSIONS

4.1. Bond along beam bar within a joint panel

The local bond stress along a beam longitudinal bar within a beam-column joint is shown in Figure 4.1 concerned with a story drift angle for Specimens Y-2 and Y-4 using deformed 19 mm and 13 mm diameter beam bars respectively. The bond stress was computed from the difference between tensile forces of a beam bar in the middle one-third region in a joint panel with a gauge length of 110 mm. Symbols of a solid circle and a open square represent the maximum bond stress and the bond stress at the peak story shear force respectively. The bond stress along the deformed 19 mm diameter bar for Specimen Y-2 reached the peak strength before the story shear force attained to a peak and hereafter bond deterioration occurred, which resulted in pinching hysteresis loops and reduction in strength due to excessive crushing in beam end concrete.

In contrast, the local bond stress along the deformed 13 mm diameter bar for Specimen Y-4 kept on increasing even after the peak story shear force was attained, which indicates that good bond along a beam longitudinal bar within a joint panel was maintained during the test. Good bond was also observed for other specimens Y-1 and Y-3 using deformed 13 mm diameter beam bars. Such good bond condition within a joint panel for these specimens led to fat spindle-shaped hysteresis loops, and the buckling of beam longitudinal bars at the beam end after the peak story shear force.

4.2. Beam Plastic Hinge

4.2.1. Distributions of beam crack width over beam length and strain along beam bar

A crack pattern at a beam deflection angle of 3.2 % corresponding to a story drift angle of 3 %, crack width distributions over a beam length at each peak of loading cycles at a beam deflection angle of 1.0 % to 4.3 %, and strain distributions along a beam longitudinal bar are shown in Figure 4.2 for the beam in Specimen Y-1. Crack widths were measured by a crack-scale at a location of a beam longitudinal bar.

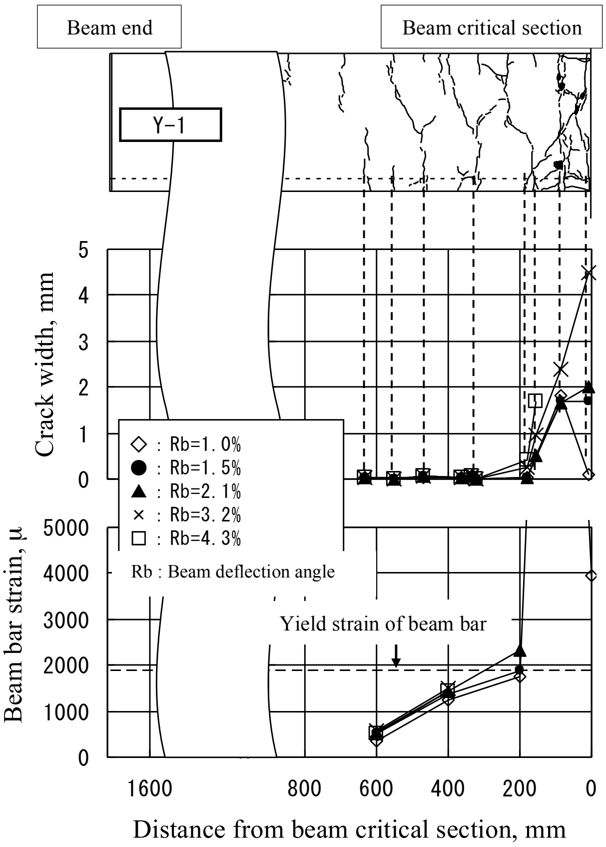

Figure 4.2. Distributions of beam crack width and beam bar strain

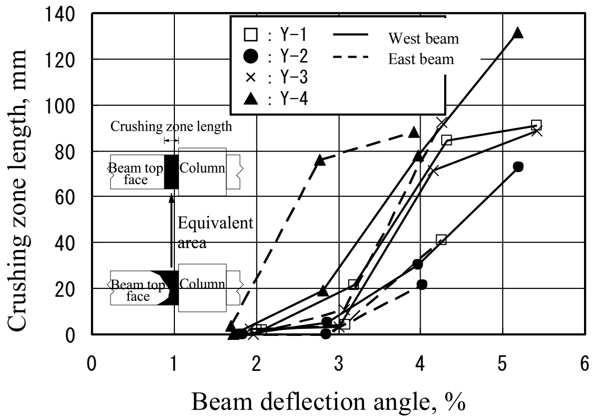

Figure 4.3. Concrete crushing zone length at beam end – beam deflection angle relationships

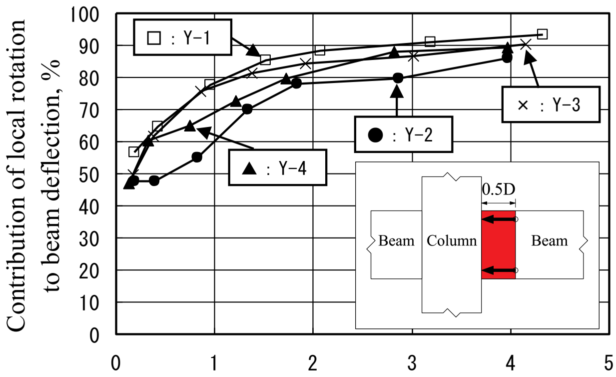

Figure 4.4. Contribution of rotation in 0.5*D* region at beam end to beam deflection

Fine cracks whose width was less than 0.1 mm and which did not almost grow with the increase in a beam deflection were observed in a region away from a distance of one-half the beam depth (designated 0.5*D* ; *D* is a beam overall depth equal to 400 mm) from a column face. Conversely, widths of cracks over a 0.5*D* distance from a column face increased with the increase in a beam deflection, attaining to 1 mm to 4.5 mm at a beam deflection angle of 3.2%. Beam longitudinal bars yielded in a region within a 0.5*D* distance from a column face. Same phenomena were also observed for other specimens. Thus a beam inelastic zone subjected to tension was located within a 0.5*D* distance from a column face for all specimens.

4.2.2. Concrete crushing zone at beam end

A length of the concrete crushing zone at a top surface of the west and east beams are shown in Figure 4.3 at each peak of loading cycles concerned with a beam deflection angle. The length was taken by the manner as follows; first the area of the concrete spall-off region on a top surface of the beam subjected to compression was found through a depiction of crack patterns, second the area was replaced by an equivalent rectangular area with a beam width, then the rectangular area divided by the beam width was regarded as the concrete crushing zone length. Although some scatter was observed for crushing zone lengths in both beams, there was a tendency to increase abruptly in the concrete crushing zone length after reaching the peak flexural capacity of the beam at a beam deflection angle of about 3 %. The greater the prestressing ratio was, the longer the crushing zone length was; Specimen Y-4 with the prestressing ratio of 0.79 had the crushing zone length 1.8 times as long as Specimen Y-2 with the ratio of 0.45 at a beam deflection angle of about 5 %. The concrete crushing zone at the beam end ranged from 0.18*D* to 0.33*D* at the end of tests, where *D* is a beam overall depth.

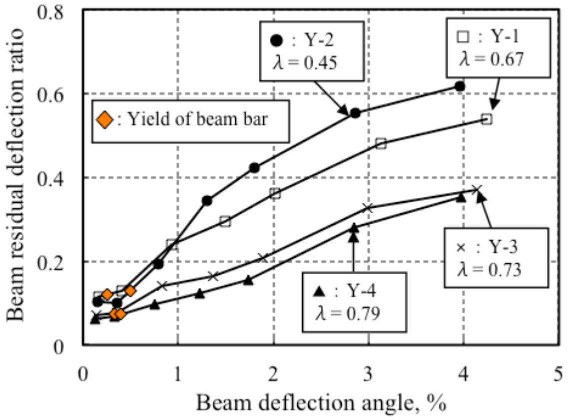

Figure 4.5. Beam residual deflection ratio - beam deflection angle relationships

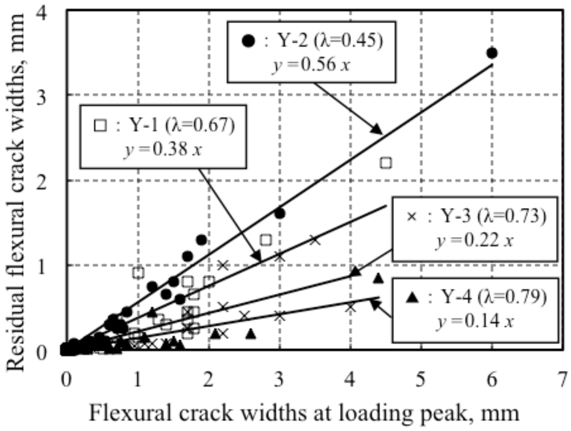

Figure 4.6. Residual flexural crack widths – flexural crack widths at loading peak relationships

4.2.3. Contribution of hinge rotation to total beam deflection

Contribution of a local rotation along a beam over a 0.5*D* distance from a column face to the beam deflection is shown in Figure 4.4 concerned with a beam deflection angle. The local rotation was obtained using axial deformations near the top and bottom surfaces of the beam measured by electric displacement transducers. The deflection component due to the local rotation increased up to a beam deflection angle of approximately 2 %, and hereafter kept almost constant, reaching 90 % and 80 % of a beam deflection angle of 3 % corresponding to the peak strength for Specimens Y-1 and Y-2 respectively. This difference of the contribution ratio was caused by a distribution of flexural and shear cracks along a beam; flexural cracks occurred sparsely in a narrow region of the beam for Specimen Y-1 whereas Specimen Y-2 had the greatest number of flexural and flexural-shear cracks along the beam. The deflection component of a 0.5*D* region at the beam end for Specimens Y-3 and Y-4 after a beam deflection angle of 3 % was almost equal to that for Specimen Y-1 and greater than that for Specimen Y-2 since a length of the concrete crushing zone at the beam end for Specimens Y-3 and Y-4 was longer than that for Specimen Y-2.

4.3. Residual Deformation and Crack Width in Beam

4.3.1. Residual deflection ratio – beam deflection angle relationships

Relationships between a beam residual deflection ratio and a beam deflection angle at each peak of loading cycles are shown in Figure 4.5. The beam residual deflection ratio was defined by the ratio of the sum of the absolute values of residual beam deflections under a positive and a negative unloading to the sum of the absolute values of peak beam deflections of a positive and a negative loading. Solid diamond-shaped symbols represent the point where beam longitudinal bars yielded. The residual deflection ratio was almost equal to 0.1 at a beam deflection angle of 0.1 % to 0.4 % for all specimens. After beam longitudinal bar yielded at a beam deflection angle of approximately 0.4 %, the residual deflection ratio begun to increase with the increase in the beam deflection, reaching 0.3 to 0.5 at a beam deflection angle of 3 %. The greater the prestressing ratio was, the smaller the residual deflection ratio was; the residual deflection ratio was the smallest for Specimen Y-4 with the prestressing ratio of 0.79 and the greatest for Specimen Y-2 with the prestressing ratio of 0.45.

4.3.2. Crack width at peak of loading cycle and unloading

Relationships between residual and peak flexural crack widths under all loading cycles are shown in Figure 4.6. Solid lines were derived from the least squares method to fit each specimen's data, whose coefficients of correlation were 0.85 to 0.99, indicating strong correlation between residual and peak flexural crack widths. A residual crack width for reinforced concrete members is commonly evaluated to be approximately 0.5 times the peak crack width (Architectural Institute of Japan 2004). Residual crack widths were 0.56 times the peak crack widths averagely, which was similar to R/C members, for Specimen Y-2 with the smallest prestressing ratio; 0.45. On the other hand, residual crack widths were merely 0.14 times the peak crack widths for Specimen Y-4 with the greatest ratio; 0.79. Thus, the greater the prestressing ratio was, the smaller the ratio of a residual crack width to a peak one became.

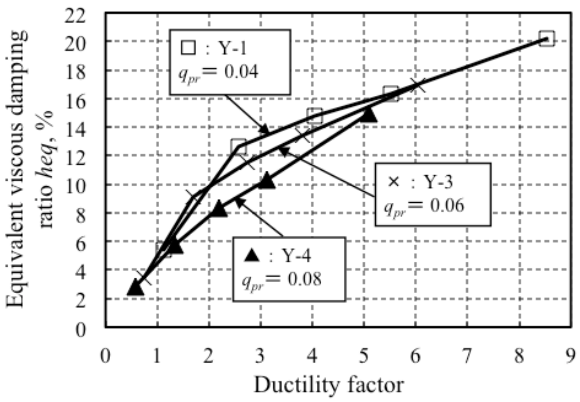

Figure 4.7. Equivalent viscous damping ratio heq – ductility factor relationships

4.4. Energy Dissipating Capacity in Beam

An equivalent viscous damping ratio, heq, for a beam of Specimens Y-1, Y-3 and Y-4, which used same 13 mm diameter deformed bars as beam longitudinal reinforcement, is shown in Figure 4.7 to investigate an energy dissipating capacity in beams. The amount of prestressing strands which is indicated by the index q_{pr} was varied among these specimens. The index q_{pr} is defined as follows.

$$q_{pr} = \frac{T_{py}+T_{po}+T_{ry}-C_{ry}}{bD\sigma_B} \tag{4.1}$$

where T_{py} , T_{ry} : tensile yield force in a prestressing strand and beam longitudinal bars at a tensile side on the beam section respectively, T_{po} , C_{ry} : effective tensile force in a prestressing strand and compressive yield force in beam longitudinal bars at a compressive side on the beam section respectively, b , D : beam width and overall depth, and σ_B : concrete compressive strength. The index q_{pr} for Specimens Y-1, Y-3 and Y-4 was 4 %, 6 % and 8 % respectively.

The abscissa of Figure 4.7 represents the ductility factor for a beam shear force – deflection relation, which is the ratio of each attained beam deflection in loading cycles to the beam yield deflection. The beam yield deflection was defined as the deflection quarter –thirds times that measured at the beam shear force three-quarters times the peak shear force, which modified the New Zealand method (e.g., Paulay and Park 1984). Equivalent viscous damping ratios for hysteresis loops where the beam shear force descended to that less than 90 percent of the peak strength were removed from Figure 4.7.

The equivalent viscous damping ratio declined with the increase in the index q_{pr}, namely, the sectional area of prestressing strands. The ratio however became a similar value of approximately 16 percent at a ductility factor of 5 to 6. This was attributed to the enhancement of energy dissipated by the concrete at a beam end where remarkable concrete crushing occurred for Specimens Y-3 and Y-4, although the origin-oriented tendency for hysteresis loops generally becomes much strong with the increase in the amount of prestressing strands.

4.5. Different Limit Sates in Beam

Envelope curves of the beam shear force – deflection angle relationship for Specimens Y-1, Y-3 and Y-4 which had each a different amount of prestressing strands are shown in Figure 4.8 with several symbols; a open diamond represents the point at beam bar yielding, open and solid triangles and a solid diamond at a residual crack width of 0.2 mm, 1.0 mm and 2.0 mm respectively, solid and open squares at a residual beam deflection angle of 0.25 % and 0.5 % respectively, solid and open circles at slight and severe crushing of beam cover concrete respectively, and x-mark at the buckling or the rupture of a beam longitudinal bar. Recommendations for each damage level of non-prestressed longitudinal bars, prestressing tendons and concrete to determine different limit states for prestressed reinforced concrete beams, proposed by Architectural Institute of Japan in 2007, are shown in Table 4.1. The beam deflection angle at which different phenomena such as beam bar yielding or concrete crushing occurred and the factor which determined different limit states are shown in Table 4.2.

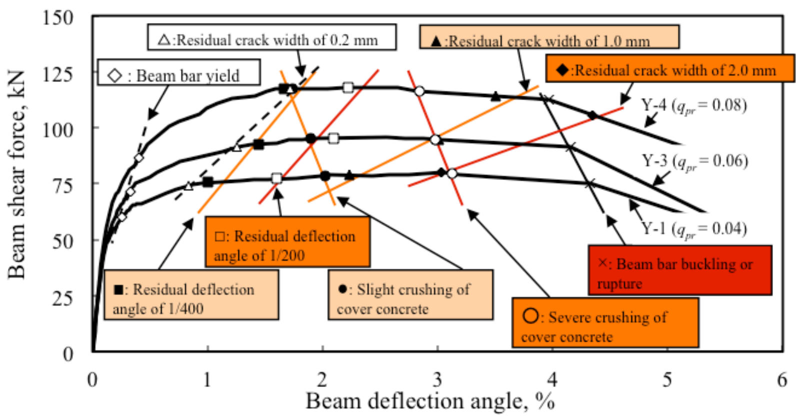

Figure 4.8. Different limit states on beam shear force – deflection angle envelope curves

Table 4.1. Recommendation for damage levels for materials to determine different limit states

Different limit states	Damage level							
	Range of prestressing ratio λ	Ordinary bar	Prestressing steel		Concrete		Residual deflection angle	Residual crack width
			Good bond	Poor bond	Usual flexural members	Other members		
Service limit state	1～0.75	Permit slight yielding.	Elastic range	Elastic range	Less than 0.9σB	Less than 0.75σB	Nearly zero	Less than 0.2 mm
	0.75～0.5		Less than strength decided by 0.2% offset		Less than (14/15λ+0.2)σB			
	Less than 0.5	Elastic range			Less than 2/3σB (σB:concrete compressive strength)			
First restorable limit state	Permit yielding.		Permit slight yielding.	Elastic range	Slight crushing of cover concrete		Less than 1/400	Less than 1.0 mm
Second restorable limit state	Longitudinal bar does not buckle.		Permit yielding.	Less than strength decided by 0.2% offset	Severe crushing of cover concrete		Less than 1/200	Less than 2.0 mm
Safety limit state	Don't buckle nor rupture.		Don't rupture.	Permit yielding.	Core concrete does not crush.		----	----

Table 4.2. Beam deflection angle at which each event occurred and factors deciding different limit states

Specimen		Y-1		Y-2		Y-3		Y-4	
Items		West beam	East beam	West beam	East beam	West beam	East beam	West beam	East beam
		Beam deflection angle, %							
Beam bar	◇ : Yielding	0.25	0.27	0.50	0.50	0.33	0.30	0.40	0.37
	× : Buckling or rupture	4.32	4.29	none	none	4.15	4.09	3.96	2.94
Concrete at beam end	● : Slight crushing of cover concrete	2.02	1.77	1.55	2.17	1.89	1.89	1.74	1.56
	O : Severe crushing of cover concrete	3.13	3.12	3.41	2.84	2.98	3.00	2.84	2.82
Residual deflection angle	■ : 1/400	1.01	1.00	0.96	0.93	1.45	1.42	1.66	1.73
	□ : 1/200	1.60	1.57	1.39	1.35	2.10	2.13	2.22	2.26
Residual crack width	△ : 0.2 mm	0.84	0.96	0.93	0.68	1.26	0.93	1.72	2.15
	▲ : 1.0 mm	2.23	1.85	1.53	2.20	3.01	2.57	3.50	3.48
	◆ : 2.0 mm	3.03	2.76	2.05	3.26			4.34	
Factor deciding each limit state	Service limit state	◇	◇	◇	◇	◇	◇	◇	◇
	First restorable limit state	■	■	■	■	■	■	■	●
	Second restorable limit state	□	□	□	□	□	□	□	□
	Safety limit state	×	×			×	×	×	×

The beam deflection angle when the residual crack width and the residual deflection angle specified to decide each limit state was attained in tests increased with the increase in the amount of prestressing strands. The beam deflection angle when concrete crushing and the buckling or the rupture of beam bars occurred at a beam end, in contrast, decreased with the increase in the amount of prestressing strands. Therefore, a first restorable limit state for Specimen Y-1 with the index q_{pr} of 4 % was reached by the residual deflection angle of 1/400 prior to the concrete slight crushing, whereas these two events occurred almost simultaneously for Specimen Y-4 with the amount of prestressing strands two times that for Specimen Y-1.

A large prestressing ratio for PRC beams causes generally concrete crushing early at a beam end. The beam deflection angles when slight and severe crushing developed at cover concrete, however, were almost equal between Specimen Y-2 with the prestressing ratio of 0.45 and Specimen Y-4 with the ratio of 0.79. The reason why the obvious difference due to the prestressing ratio for the occurrence of concrete crushing was not observed is because concrete crushing was induced by bond deterioration along beam longitudinal bars within a joint panel for Specimen Y-2 using 19 mm diameter beam bars.

For all beams shown in Table 4.2, a service limit state was reached by yielding of non-prestressed beam bars at a beam deflection angle of 0.25 % to 0.50 %, a first restorable limit state by the residual deflection angle of 1/400 at a beam deflection angle of 0.93 % to 1.66 %, and a second restorable limit state by the residual deflection angle of 1/200 at a beam deflection angle of 1.35 % to 2.26 %. A safety limit state was reached by the buckling or the rupture of beam bars at a beam deflection angle of 2.94 % to 4.32 % except for Specimen Y-2, where the safety limit state was not observed in the test.

5. CONCLUSIONS

Concluding remarks drawn by this study are as follows.

(1) Relationships between story shear force and story drift exhibited fat spindle-shaped hysteretic loops for specimens using deformed 13 mm diameter beam bars, and buckling and rupture of beam longitudinal bars eventually occurred. These were caused by good bond along beam longitudinal bars within a beam-column joint. In contrast, a specimen, using deformed 19 mm diameter beam bars and with a contribution ratio of PC tendons to ultimate flexural capacity of a beam section of 0.45, showed pinching hysteresis loops such as observed in R/C structures and concrete crush at a beam end.

(2) A plastic hinge length at a beam end region was regarded as one-half the depth of a beam section for all specimens by following facts. First, flexural crack widths became large and beam longitudinal bars yielded with the increase in beam deflection within the region. Second, deformation due to local rotation in a region with a length of half a beam depth at a beam end shared eighty to ninety percent of total beam deflection at a beam deflection angle of 3 % which corresponded to beam flexural capacity.

(3) A concrete crushing region at a beam end became wide with the increase in a contribution ratio of PC tendons to ultimate flexural capacity of a beam section. For instance, the length of concrete crushing region at the end of the beam with a contribution ratio of PC tendons to ultimate beam flexural capacity of 0.79 was 1.8 times as great as that for the specimen with the contribution ratio of 0.45. The concrete crushing region length reached eventually 0.18 to 0.33 times the beam depth.

(4) The greater a contribution ratio of PC tendons to ultimate flexural capacity of a beam section was, the smaller residual deformation of a beam was. A ratio of residual flexural crack width to that at the loading peak was approximately 0.5 like R/C members when a contribution ratio of PC tendons to ultimate flexural capacity of a beam section was 0.45 whereas the residual ratio of crack width reduced to 0.14 when the contribution ratio of PC tendons was 0.79.

(5) A beam deflection angle corresponding to each limit state was 0.25% to 0.50 % at a service limit state, 0.93% to 1.66 % at a first restorable limit state, 1.35% to 2.26 % at a second restorable limit state and 2.94% to 4.32 % at a safety limit state.

(6) Energy dissipating capacity of a PRC beam during earthquake excitation showed a tendency to decrease with the increase in an amount of sectional area of prestressing tendons.

AKCNOWLEDGEMENT

A part of the study described herein was sponsored by the Grant-in-aid for Scientific Research (C) of Japan Society for the Promotion of Science (Researcher : KITAYAMA K.). Authors would like to express their gratitude to Tokyo Tekko Co. Ltd. for providing steel bars, Dr. MINAMI S., assistant professor of Tokyo Metropolitan University and PS Mitsubishi Co. Ltd. for their assistance in conducting the tests.

REFERENCES

Architectural Institute of Japan. (2004), Guidelines for Performance Evaluation of Earthquake Resistant Reinforced Concrete Buildings (Draft), Architectural Institute of Japan. (in Japanese)

Paulay, T. and R. Park (1984). Joints in Reinforced Concrete Frames Designed for Earthquake Resistance. Research report 84-9, University of Canterbury.